Mathematical Biosciences and Engineering, 16(3): 1597–1610.
DOI: 10.3934/mbe.2019076
Received: 22 December 2018
Accepted: 27 January 2019
Published: 26 February 2019

http://www.aimspress.com/journal/MBE

Research article

Minimally invasive treatment of calcaneal fractures via the sinus tarsi approach based on a 3D printing technique

Lufeng Yao[1,†], Haiqing Wang[1,†], Feng Zhang[1,*], Liping Wang[2,3,*] and Jianghui Dong[2,3,*]

[1] Department of Foot and Ankle Surgery, Ningbo No. 6 Hospital, Ningbo, 315040, China
[2] Department of Hand Surgery, Department of Plastic Reconstructive Surgery, Ningbo No. 6 Hospital, Ningbo, 315040, China
[3] School of Pharmacy and Medical Sciences, University of South Australia, Adelaide, SA 5001, Australia

* **Correspondence:** Email: fazhang189@hotmail.com, liping.wang@unisa.edu.au, jianghui.dong@unisa.edu.au; Tel: +86-0574-87996063, +86-0574-87775162, +61-883022715; Fax: +86-0574-87809785, +86-0574-8780978, +61-883021087.

† These two authors contributed equally.

Abstract: The sinus tarsi approach can be used for a limited exposure of the calcaneal fracture site. The reduction of the posterior articular surface, the shape of the calcaneus, the precise placement of the sustentacular screw (SS), the posterior articular surface screw of the calcaneal (PASS), and the long axis screw of the calcaneal (LAS) are still challenging. To that end, we proposed a minimally invasive technique for the treatment of calcaneal fractures via the sinus tarsi approach in combination with a three-dimensional (3D) printing technique. First, a 3D reconstructed model of the bilateral calcanei was obtained according to the computed tomography (CT) scan data and was used to simulate the placement of screws and acquire the screw trajectory parameters. Next, using 3D printing, a model of the calcaneus was printed, and the minimally invasive steel plate was pre-shaped to fit the lateral wall of the model. Finally, a total of 25 patients underwent this procedure. The results showed significant accuracy improvement in terms of the SS, PASS and LAS placement and in terms of the parameters including Bohler's angle, Gissane's angle, and the calcaneal width. In this work, the technique of the personalized minimally invasive treatment of calcaneal fractures improved the accuracy of screw placement (SP) and the reduction rate of posterior articular surface, improved the shape of the calcaneus, and increased the precision of the minimally invasive treatment of calcaneal fractures via the sinus tarsi approach.

Keywords: calcaneus fracture; minimally invasive; 3D printing; sinus tarsi approach; screw trajectory

1. Introduction

Calcaneal fractures account for approximately 60% of tarsal bones fractures [1,2] The traditional extended lateral calcaneal approach can be used to clearly expose the posterior articular surface fracture and the lateral wall of the calcaneus for reduction under direct vision. However, the complication rate is as high as 37%, and the infection rate is approximately 20% [1,3]. To reduce the incision complications and the infection rate of calcaneal fractures, the new minimally invasive treatment techniques have emerged successively [4–7]. However, the minimally invasive techniques have limited exposure and are unable to be used for articular surface reduction under direct vision [8,9]. Potential complications, such as poor articular surface reduction, malunion, and loss of reduction may occur [10,11].

To date, the challenges of minimally invasive calcaneal fracture treatment lie in the following: ① how to improve the reduction rate of the posterior articular surface and improve the shape of the calcaneus; and ② how to improve the accuracy in the placement of the SS, the LAS, and the PASS. The sinus tarsi approach can be used to expose the operative field and to protect the soft tissue. This approach is the current popularized surgical method for the minimally invasive treatment of calcaneal fractures [11–13]. During the reduction and internal fixation via the sinus tarsi approach, the sustentaculum tali is an important reference point for the reduction of intra-articular fractures of the calcaneus [14,15]. However, the SS can only be placed indirectly from the lateral side to the medial side [16], the screw trajectory is narrow, and the success rate of SS placement is not high [16–19].

To improve the reduction rate of the posterior articular surface and the shape of the calcaneus fracture, and the SS, LAS and PASS placement success rate, we proposed a minimally invasive treatment of calcaneus fractures via the sinus tarsi approach based on a 3D printing technique. Currently, the application of 3D printing technology is rarely reported in the field of ankle surgery, especially in the case of the minimally invasive treatment of calcaneal fractures [20–23].

The aims of the current work were: ① The 3D reconstruction calcaneal model will be obtained, and the optimal screw trajectory will be designed on the calcaneus model to determine the individualized parameters of SP. ② The model of the calcaneus will be printed using 3D printing, and the minimally invasive steel plate will be pre-shaped to fit the lateral wall of the model. ③ According to the determined parameters for SP, minimally invasive surgery of the calcaneal fracture will be performed including fabrication of the steel plate and SP. Finally, postoperative evaluations will be performed to verify the accuracy of the SP.

2. Materials and methods

The current work was reviewed and approved by the Ethics Committee of the Ningbo No. 6 Hospital. The patients reviewed the written surgical plan and alternative regimen before the procedure and signed the informed consent form.

2.1. Minimally invasive treatment of calcaneal fracture via sinus tarsi approach

The minimally invasive treatment via the sinus tarsi approach is divided into two sections: the reduction of the posterior articular calcaneus surface, and the precise placement of the SS, LAS and PASS (Figure 1).

First, the sinus tarsi approach was used to expose the posterior calcaneus articular surface and to protect the superficial peroneal nerve and sural nerve. Then, the displacement of the calcaneus was reduced by manipulation. Intraoperative fluoroscopy was performed to verify the fitness of the pre-shaped minimally invasive steel plate to the lateral wall of the calcaneus. If the plate fitted, the reduction of calcaneus posterior articular surface and shape was considered to be satisfactory. If it did not fit, the further reduction was required.

Second, the SS, LAS, and PASS were placed precisely. First, the screw entry points and exit points of the SS, LAS, and PASS at the lateral wall of the calcaneus and the calcaneal tuberosity were determined. Next, the angle of the screw insertion and the length of the screw trajectory were determined. Finally, the screws were placed one by one to complete the internal fixation of the calcaneus fracture.

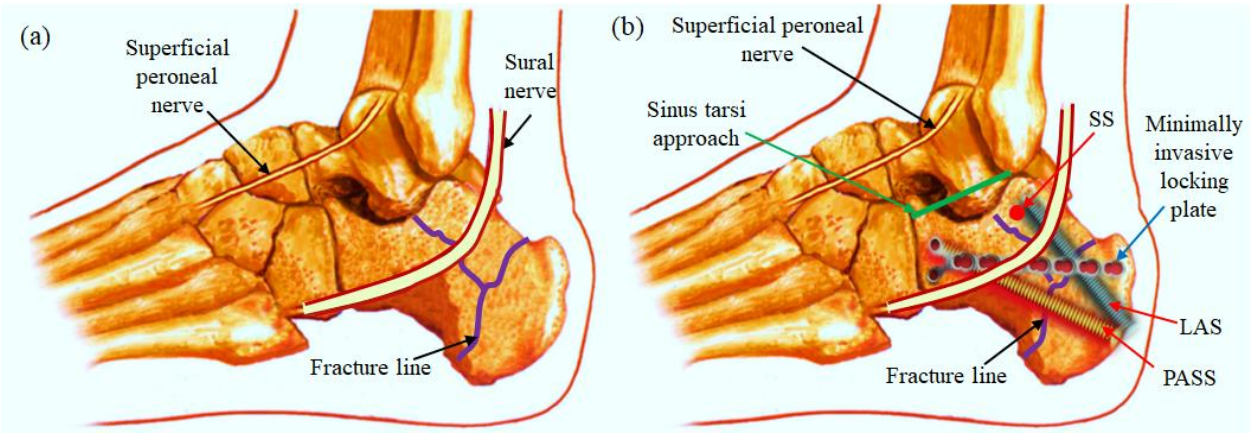

Figure 1. Minimally invasive treatment of calcaneal fracture via the sinus tarsi approach. (a) Preoperative anatomical structures and relationship to the adjacent structures. (b) Internal fixation of the calcaneal fracture.

2.2. 3D modeling of the calcaneus and 3D printing

The patient's bilateral calcanei was scanned using CT (Philips Brilliance 64 CT, Philips Medical Systems, Netherlands) with a slice thickness of 1 mm and a slice interval of 0.5 mm. The CT data were imported into MIMICS 15.0 (Meterialise, Leuven, Belgium) for 3D reconstruction. The 3D reconstruction model of the calcaneus is shown in Figures 2a–c.

The STL formatted data of the 3D reconstruction model of the affected calcaneus and the mirror model of the contralateral calcaneus were imported into the Makerbot replicator 3D printing device (Makerbot, USA) to obtain a printed 3D model (Figures 2d, e).

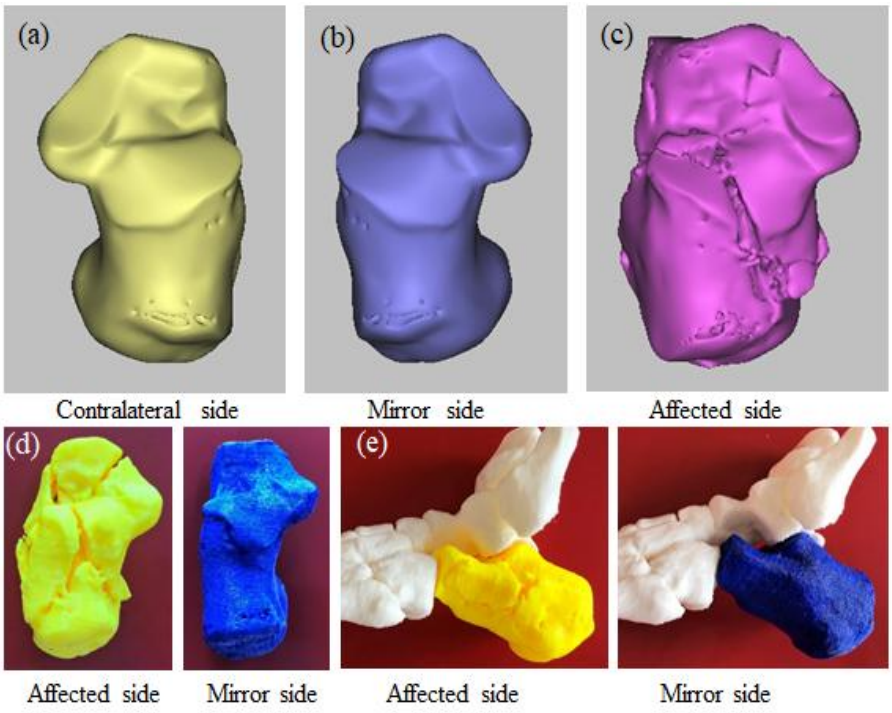

Figure 2. 3D modeling of the calcaneus and 3D printed models. (a) The contralateral calcaneus. (b) The mirror model of the contralateral calcaneus. (c) The affected calcaneus. (d) The affected calcaneus and the mirror model of the contralateral calcaneus. (e) 3D printing of the affected calcaneus and the mirror-model calcaneus.

2.3. Surgical design

MIMICS software was used to simulate SP on the 3D model of the mirror-image calcaneus.

First, the SS, PASS and LAS entry and exit points were determined. Then, the maximum trajectory lengths, L_{SS}, L_{PASS}, and L_{LAS}, were determined. The trajectories of SS, PASS, and LAS placement were adjusted individually to ensure no involvement of the subtalar articular surface during SS placement, no penetration of the medial wall and posterior articular surfaces of the calcaneus during PASS placement, and no penetration of the lateral wall and the calcaneocuboid joint during LAS placement. Next, the interference of the three screw trajectories was assessed. If interference was identified, the screw trajectories were adjusted until there was no sign of interference. Finally, the actual SP angles were determined for application during the procedure. The angles between the PASS, LAS, and SS and the horizontal plane and the angles between the PASS, LAS, and SS and the coronal plane were obtained and expressed, respectively, as follows: α_{PASS} and β_{PASS}; α_{LAS} and β_{LAS}; α_{SS} and β_{SS} (Figures 3a–g).

In the 3D printed model, the SS, LAS, and PASS entry points were designed. The simulated procedure was performed according to the depth and angle of the screw insertion determined by the simulated SP. Finally, the minimally invasive steel plate was pre-shaped to fit the lateral wall of the calcaneus and fixed to the model (Figures 4a–d).

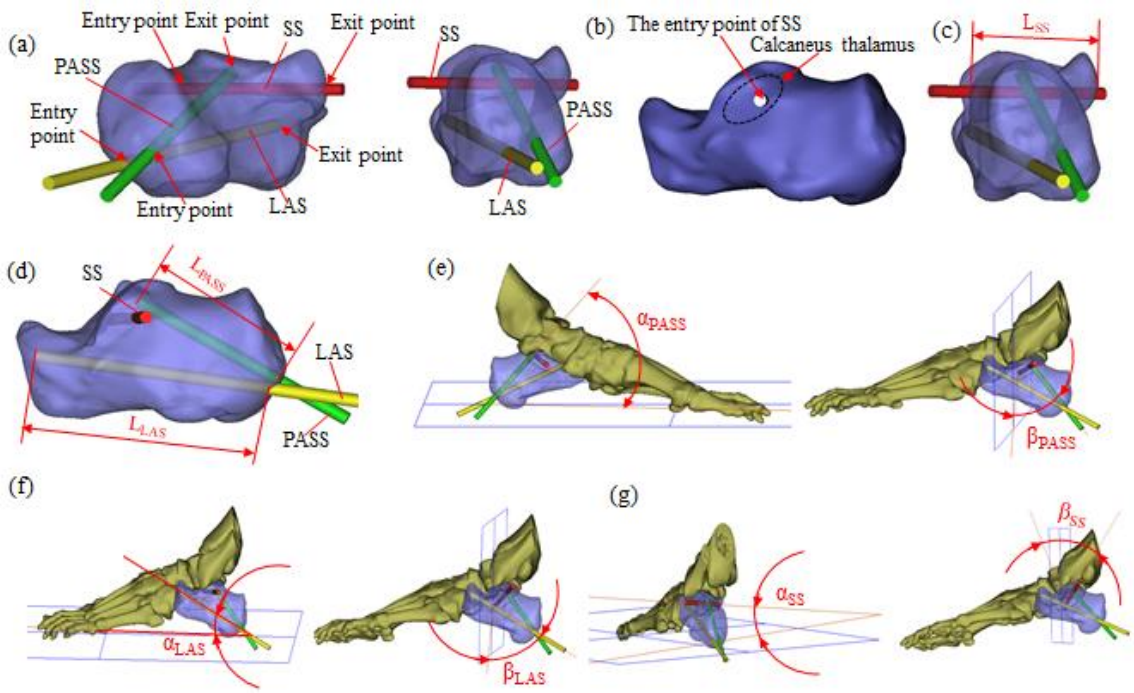

Figure 3. The design of the screw trajectory using the 3D model. (a) SS entry point (posterior-inferior to the calcaneus thalamus portion) and exit point (center of the sustentaculum tali); PASS entry point (medial calcaneal tuberosity) and exit point (center of the posterior articular surface); LAS entry point (lateral calcaneal tuberosity) and the exit point (the center of the anterior process of the calcaneus). (b) SS entry point. (c) The maximum length of SS, L_{SS}. (d) The maximum lengths of trajectories, L_{PASS} and L_{LAS}. (e) The angle α_{PASS} is between the PASS and the horizontal plane and the angle β_{PASS} is between PASS and the coronal plane. (f) α_{LAS} is the angle between the LAS and the horizontal plane and β_{LAS} is the angle between the LAS and the coronal plane. (g) α_{SS} is the angle between the SS and the horizontal plane and β_{SS} is the angle between the SS and the coronal plane.

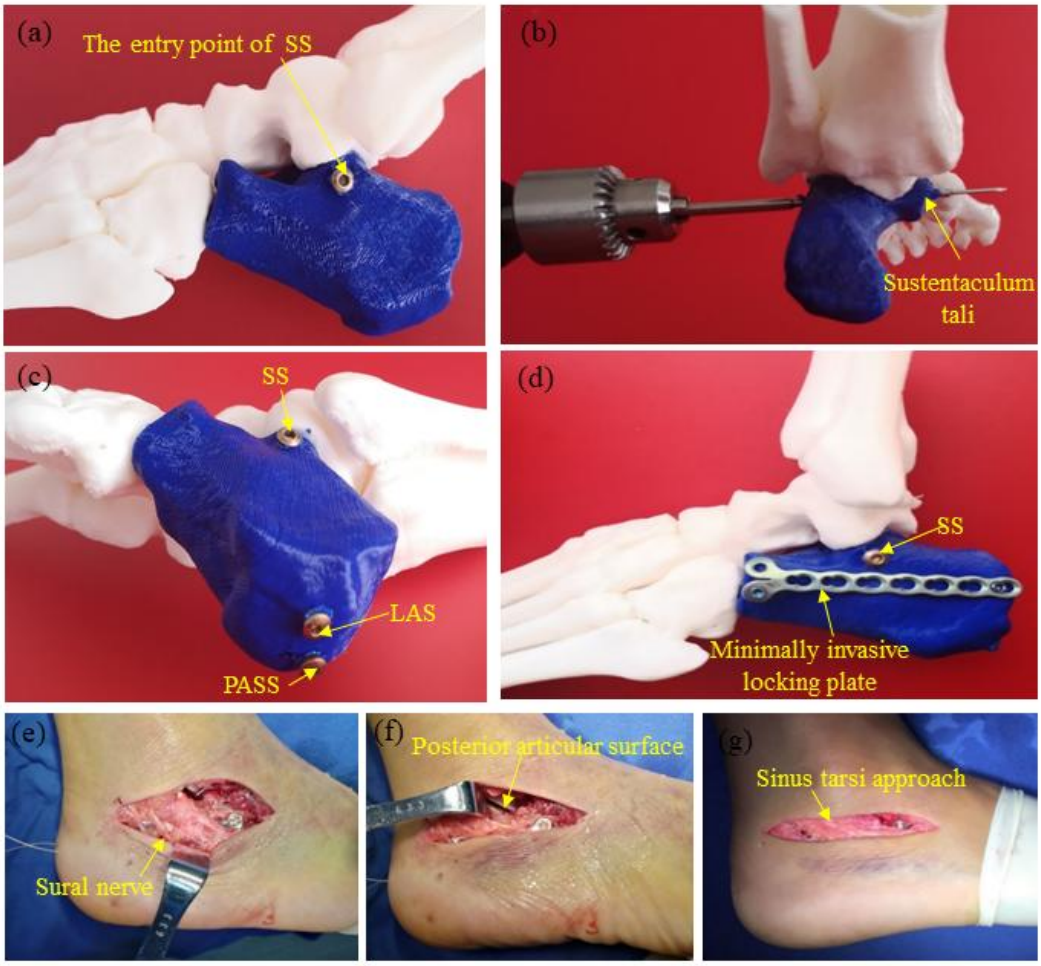

Figure 4. Simulation of the procedure and intraoperative operation. (a) Determination of the SS entry point. (b) SS placement on the 3D printed model. (c) The LAS and PASS entry points. (d) Pre-shape of the minimally invasive steel plate. (e) Avoidance of sural nerve injury during surgery. (f) Intraoperative reduction of the posterior articular calcaneus surface under direct vision. (g) Postoperative sinus tarsi incision.

2.4. Intraoperative procedure

First, a periosteal stripper was used to manipulate the medial fracture fragment of the calcaneus at the fracture line for reduction. Then, a Kirschner wire was used to transversely cross through the calcaneus tuberosity for lateral traction to correct the calcaneal varus and restore the length of the calcaneus. Finally, the fracture fragment of the lateral wall of the calcaneus was reduced under direct vision and temporarily fixed with the Kirschner wire (Figures 4e, f). The pre-shaped minimally invasive steel plate was placed on the lateral wall of the calcaneus. If it fitted, the reduction of the posterior articular surface and the shape restoration of the calcaneus were considered satisfactory.

The SS, PASS, and LAS were placed in sequence. The pre-shaped minimally invasive steel plate was then fixed to the lateral wall of the calcaneus. Fluoroscopy was used to confirm that the reduction of the posterior articular surface and the shape restoration of the calcaneus were satisfactory and that the force line was restored (Figure 4g). A drainage tube was placed in the

incision site. The incision was closed in layers and dressed with a sterile compression bandage.

2.5. Postoperative evaluation

The Bohler's angle (B_2), the Gissane's angle (G_2), and the calcaneus width (W_2) were measured in the lateral and axial view of the heel after surgery. Postoperative CT scans with 3D reconstruction were performed to compare the preoperative and postoperative data to determine the accuracy of the SS, LAS, and PASS placements. Furthermore, the Kurozumi [24] grading system was used to evaluate the articular surface reduction. The patient's incision complications were recorded after surgery, and the patient's the American Orthopedic Foot and Ankle Society (AOFAS) [25] score and visual analog scale (VAS) [26] score were evaluated at the final follow-up visit.

2.6. Application

From June 2016 to February 2017, 25 patients underwent the proposed procedure. The patients were 20 to 59 years of age, with an average age of 43 years (Table 1). Patients with Sanders type-II and simple Sanders type-III fractures of the calcaneus were included.

Table 1. Patient demographic data.

Case	Sex	Cause of injury	Smoking	Sanders Classificati0n	Preoperative preparation (days)	Operative time (minutes)	Length of hospital stay (days)	Follow-up period (months)	Complications	AOFAS score	VAS score
1	F	Fall	N	III	4	70	8	17	None	90	0
2	M	Fall	Y	II	5	68	9	16	None	92	2
3	M	Fall	Y	III	5	66	10	13	None	92	2
4	M	Fall	N	II	5	70	9	14	None	89	3
5	M	Fall	Y	II	4	65	9	6	None	90	2
6	M	Fall	Y	III	5	75	9	11	None	100	0
7	M	Fall	N	II	6	58	10	10	None	92	1
8	F	Fall	N	II	5	60	11	12	Incisional Numbness	86	1
9	M	Fall	N	II	6	68	10	14	None	87	4
10	M	Fall	Y	III	5	66	9	18	Incisional infection	98	0
11	M	Fall	N	III	6	60	11	20	None	90	1
12	M	Fall	Y	II	5	67	7	12	None	92	1
13	M	Fall	N	II	4	60	8	16	None	98	0
14	M	Fall	N	II	5	72	9	15	Incisional numbness	86	4
15	M	Fall	N	III	4	70	7	19	None	89	3
16	M	Fall	Y	II	5	65	8	14	None	90	2

Continued on next page

Case	Sex	Cause of injury	Smoking	Sanders Classificati0n	Preoperative preparation (days)	Operative time (minutes)	Length of hospital stay (days)	Follow-up period (months)	Complications	AOFAS score	VAS score
17	F	Fall	N	II	5	69	11	18	None	92	1
18	M	Fall	Y	III	5	57	10	13	None	85	2
19	M	Fall	N	II	5	68	9	10	None	86	4
20	M	Fall	N	II	4	66	10	8	None	88	3
21	M	Fall	N	II	4	70	8	17	None	92	2
22	M	Fall	Y	III	5	72	9	18	None	92	1
23	F	Fall	Y	II	5	58	11	16	None	100	0
24	M	Fall	Y	III	5	78	10	20	Incisional infection	95	4
25	M	Fall	N	II	4	67	9	12	None	97	0

The follow-up measurement showed that the Bohler's angle (B_2), the Gissane's angle (G_2), and the calcaneus width (W_2) of the calcaneus in the lateral and axial view of the heel returned to normal after surgery suggesting that the posterior articular surface and shape of the calcaneus returned to normal.

After surgery, the average AOFAS score was 91.5 points (range: 85–100). The average postoperative average VAS score was 1.7 points (range: 0–4 points). Only 2/25 (8%) of the patients had superficial incision infections and recovered after changing the incision dressing, and 2/25 (8%) patients had numbness and discomfort in the lateral margin of the foot and recovered spontaneously approximately 3 months after surgery.

3. Results

3.1. Typical case of Sanders type-II calcaneal fracture

A 46-year-old female presented with a Sander II comminuted fracture of the right calcaneus caused by a fall from a height. Simulated SP: (1) the maximum length of each screw trajectory was listed as follows: L_{PASS} = 46 mm, L_{LAS} = 70 mm, and L_{SS} = 46 mm. (2) the angles of the screw insertion were shown as follows: $\alpha_{PASS} = 54^{\circ}$, $\beta_{PASS} = 36^{\circ}$, $\alpha_{LAS} = 29^{\circ}$, $\beta_{LAS} = 61^{\circ}$, $\alpha_{SS} = 8^{\circ}$, and $\beta_{SS} = 16^{\circ}$.

Postoperative fluoroscopy indicated that the size and shape of the calcaneus returned to normal. Postoperative CT showed a good reduction of the subtalar articular surface and accurate placement of each screw. No complications occurred during follow-ups. In the final follow-up visit, the AOFAS score was 94 points, and the VAS score was 2 points. Six months after surgery, the patient had returned to his daily work with well-recovered function (Figure 5).

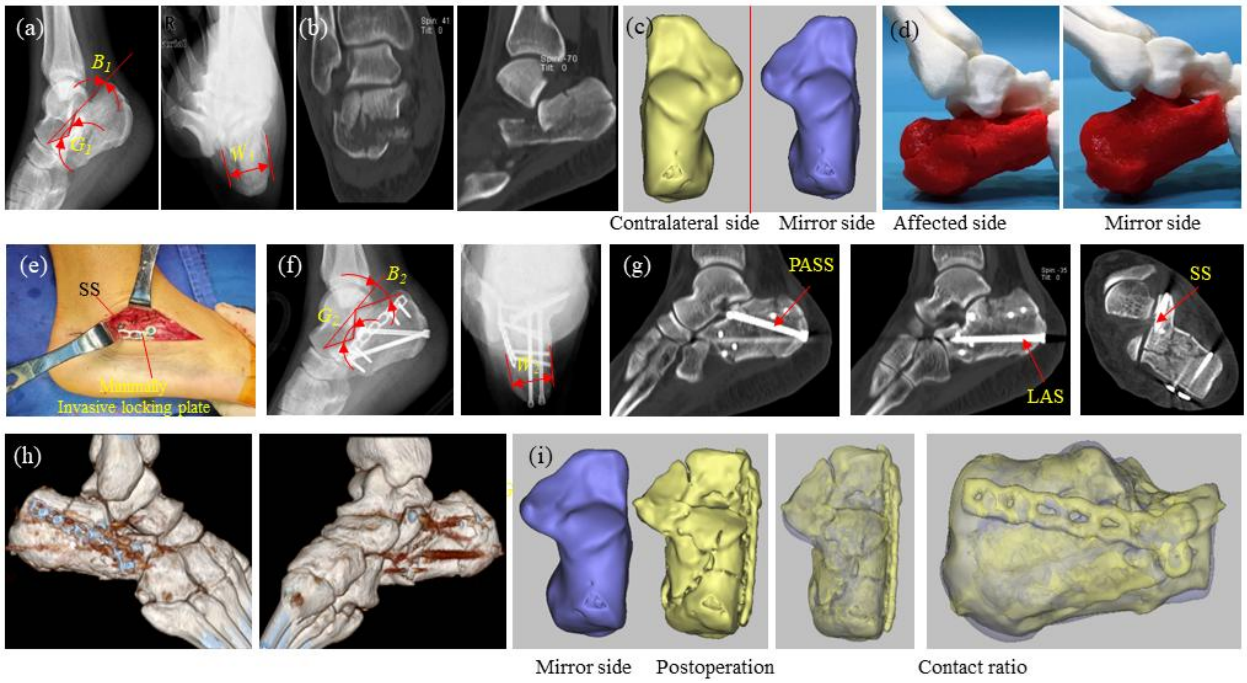

Figure 5. Typical case of Sanders type-II calcaneal fracture. (a) Preoperative measurement in the lateral and axial view of the heel, G_1 = 140°, B_1 =0°, W_1 = 45.4 mm. (b) Preoperative coronal and sagittal CT. (c) Preoperative calcaneal modeling. (d) 3D printing of the models of the contralateral mirror-image calcaneus and the affected calcaneus. (e) During surgery: the SS entrypoint and the minimally invasive steel plate for the calcaneus. (f) After surgery: Follow-up measurement in the lateral and axial view of the heel showing G_2 = 111°, B_2 = 22°, W_2 = 35.7 mm. (g) Postoperative follow-up CT of the calcaneus. (h) Postoperative 3D reconstruction. (i) Assessment of postoperative fracture contact ratio.

3.2. Typical case of Sanders type-III calcaneal fractures

A 55-year-old female presented with Sanders type-II comminuted fracture of the right calcaneus due to fall from a tree. Fluoroscopy showed the collapsed calcaneal articular surface and the widened calcaneus. The simulated surgical plan was given as follows: (1) the maximum length of each screw trajectory was shown the following: L_{PASS} = 48 mm, L_{LAS} = 75 mm, and L_{SS} = 46 mm. (3) the angles of the screw insertion were listed as follows: α_{PASS} = 48°, β_{PASS} = 33°, α_{LAS} = 25°, β_{LAS} = 64°, α_{SS} = 11°, and β_{SS} = 20°.

Postoperative fluoroscopy indicated that the shape of the calcaneus returned to normal. Postoperative CT showed a good reduction of each articular surface and accurate placement of each screw. The patient's incision healed well, and there was no complaint of discomfort after surgery. Comparing the contralateral mirror-image calcaneal model with the postoperative calcaneus model, the axial and lateral contact ratio was high. It was indicated that the shape of the affected calcaneus returned to normal. In the final follow-up, the AOFAS score was 92 points, and the VAS score was 2 points. Five months after surgery, the patient walked freely with well-recovered function (Figure 6).

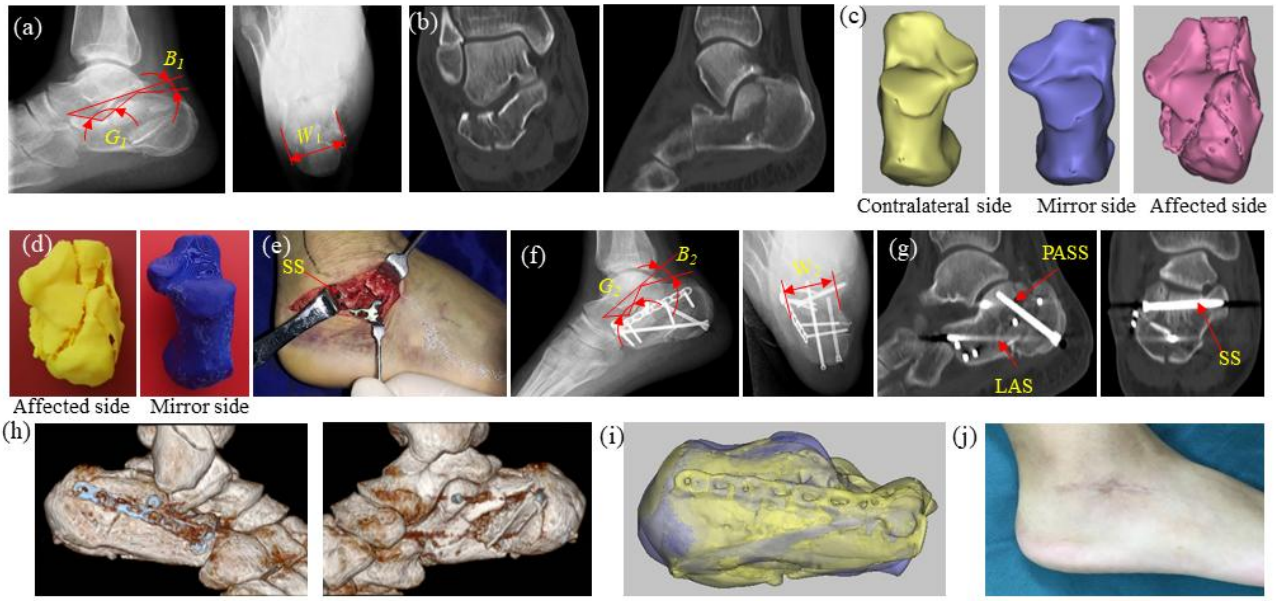

Figure 6. Typical cases of Sanders type-III calcaneal fracture. (a) Preoperative measurement of the lateral and axial view of the heel showed G_1 = 150°, B_1 = 13°, and W_1 = 47.4 mm. (b) Preoperative coronal and sagittal CT. (c) Preoperative calcaneal modeling. (d) 3D printing of the contralateral mirror-image calcaneus and the affected calcaneus models. (e) During surgery: the SS entry point and the minimally invasive steel plate for the calcaneus. (f) Postoperative measurement of the lateral and axial view of the heel showing G_2 = 120°, B_2 = 28°, and W_2 = 36.5 mm. (g) Postoperative follow-up CT of the calcaneus. (h) Postoperative 3D reconstruction. (i) Postoperative contact ratio was evaluated. (j)The sinus tarsi incision healed well 2 weeks after surgery.

3.3. CT evaluation

The evaluation of the articular surface reduction showed excellent recovery in 11 patients, good recovery in 9 patients, fair recovery in 5 patients, and poor recovery in no patients. The evaluation of the reduction of the articular surface of the calcaneocuboid joint showed good recovery in 14 patients, fair recovery in 11 patients, and poor recovery in no patients. Only 1 patient (4%) had a loss of reduction of the posterior calcaneus articular surface. The reduction rate of the posterior calcaneus surface was 96%. In the past, 2D conventional radiography was used to evaluate calcaneal fracture. However, CT is the main and effective tool to evaluate calcaneal fracture classification systems. Because CT can demonstrate better characterization and visualization of fragment displacement and fracture lines.

4. Discussion

Minimally invasive treatment via the sinus tarsi approach is a difficult operation, and the sural nerve is easily damaged during surgery due to the limited exposure in the sinus tarsi incision [20]. The difficulties of the procedure included the restoration of the calcaneus posterior articular surface and the precise orientation of the SS, LAS, and PASS. Here, we proposed a personalized minimally

invasive treatment of calcaneal fractures via the sinus tarsi approach using 3D printing technology. Preoperatively, the 3D model of the calcaneus was printed for each individual and used for pre-shaping the minimally invasive calcaneus steel plate and for the surgery simulation. During surgery, the pre-shaped steel plate was used to evaluate the reduction of the calcaneal fracture by fitting the plate to the calcaneus. Here, we improved the SP accuracy, improved the reduction rate of the posterior articular surface, restored the shape of the calcaneus, and increased the precision of the minimally invasive treatment of calcaneal fractures via the sinus tarsi approach.

The screw trajectory was designed on the reconstructed 3D model, and the simulated procedure was performed on the 3D printed model. These steps improved the success rate of SS, LAS, and PASS placement and reduced the iatrogenic injury caused by the failure of SP [27,28]. Accurate insertion of the screw restores and maintains the height, width, articular surface, and force line of the calcaneus to achieve a strong internal fixation [15]. The calcaneus thalamus portion and the calcaneal tuberosity are the structures that include cross-linked trabecular bones, which are hard and can remain intact in calcaneal fractures. Therefore, we chose the posterior-inferior site of the calcaneus thalamus portion as the SS entry point and had the PASS and LAS entry points at the medial and lateral sides of the calcaneus tuberosity, respectively. The SP parameters obtained using the 3D reconstructed model were used to guide the SP during surgery and can greatly improve the accuracy of the SP. At the same time, the length of the guide wire and the maximum length of the screw trajectory were compared during the operation to assess the initial accuracy of the SP. In summary, these preoperative simulations and intraoperative operations guarantee improved success rates in terms of SS, PASS, and LAS placement.

The success rate of SS placement in this study is significantly greater than that in traditional SS placement, as shown in Figure 7. Geerling et al. [29] used 3D image navigation technology to guide SP, and the success rate of SS placement was 24/32 (75%). Wang et al. [18] designed a SS-guiding device to assist SS placement, and the SS placement success rate in 10 cadaver specimens was 35/40 (87.5%). Here, postoperative CT findings showed that in 22 cases, SS were accurately placed in the sustentaculum tali, and in 3 cases, SS were placed in the bone of the base of the sustentaculum tali. No medial vessel, nerve, or tendon injury occurred. In 24 patients, the PASS trajectory was parallel with the lateral wall of the calcaneus and perpendicular to the posterior calcaneus articular surface but did not penetrate the posterior calcaneus articular surface or the medial wall of the calcaneus. In one patient (Case 3), PASS went through the edge of the posterior articular surface of the calcaneus. No treatment was required because the patient had no symptoms. In 23 patients, the LAS were accurately placed in the calcaneus protrusion, and in two patients (Cases 8 and 20), the LAS were placed in the bone below the anterior process of the calcaneus. There was no case of involvement of the lateral bone cortex or the calcaneocuboid joint.

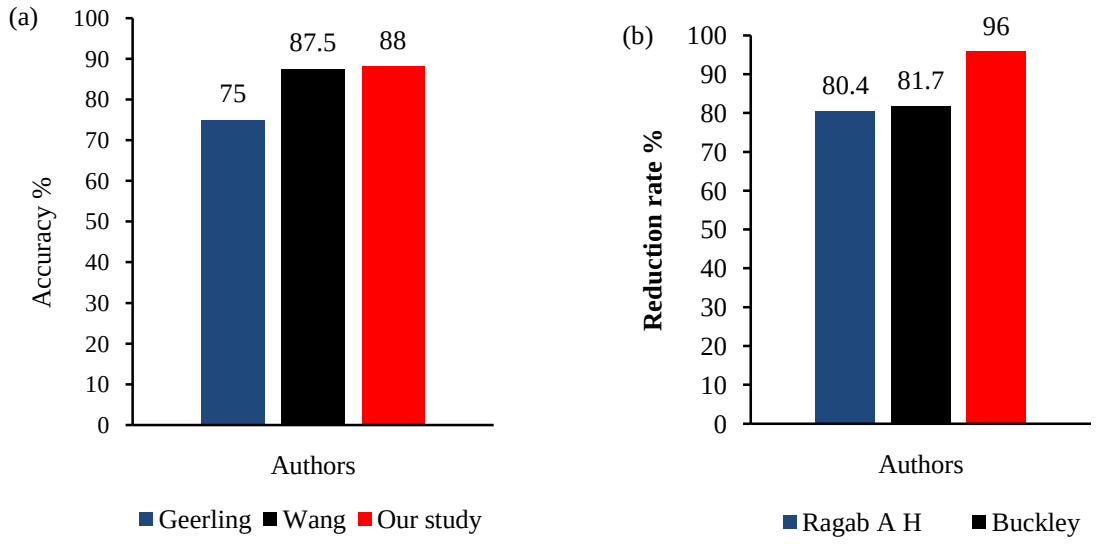

Figure 7. SS SP accuracy and posterior calcaneus articular surface reduction rate. (a) SS SP accuracy. (b) The reduction rate of the posterior articular surface of the calcaneus.

In this study, the reduction of the posterior calcaneal articular surface after calcaneus fracture was satisfactory with a greater posterior calcaneus articular surface reduction rate than when using the traditional method (Figure 7). Zhang et al. [10] compared the sinus tarsi incision with the longitudinal incision and revealed that the postoperative intra-articular steps after treatment via the sinus tarsi incision in patients with Sanders type-II and Sanders type-III fractures were 1.0 mm and 1.2 mm, respectively. In the study by Buckley et al. [30], postoperative CT was used to measure the posterior articular step and showed the step was no larger than 2 mm in 81.7% of patients. The reduction rate of the posterior calcaneus articular surface reported by Ragab et al. [31] was 37/46 (80.4%). In our work, only 4% of patients had loss of posterior calcaneus articular surface reduction, and there was no loss of reduction in the articular surface of the calcaneocuboid joint. The reduction rate of the posterior articular surface was 96%. Obviously, the reduction rate of the posterior calcaneus articular surface was greater in this study than in previous studies. These results suggest that the pre-shaped minimally invasive steel plate on the personalized 3D-printed model can improve the reduction rate of calcaneal fracture.

Acknowledgements

This work was supported by Australian National Health and Medical Research Council (NHMRC) Fellowship (1158402) and National Natural Science Foundation of China (NSFC) project (81671928), Ningbo Science & Technology Program on Social Development (2017C50048, 2016A22). LPW is supported by NHMRC Fellowship (1158402) and NSFC (81671928).

Conflicts of interest

The authors declare no conflict of interest.

References

1. N. Gougoulias, A. Khanna and D. J. McBride, et al., Management of calcaneal fractures: Systematic review of randomized trials, *Brit. Med. Bull.,* **92** (2009), 153–167.
2. N. Epstein, S. Chandran and L. Chou, Current concepts review: Intra-articular fractures of the calcaneus, *Foot. Ankle. Int.,* **33** (2012), 79–86.
3. M. J. Gardner, S. E. Nork and D. P. Barei, et al., Secondary soft tissue compromise in tongue-type calcaneus fractures, *J. Orthop. Trauma.,* **22** (2008), 439–45.
4. T. Tomesen, J. Biert and J. P. Frolke, Treatment of displaced intra-articular calcaneal fractures with closed reduction and percutaneous screw fixation, *J. Bone. Joint. Surg. Am.,* **93** (2011), 920–928.
5. B. S. Sivakumar, P. Wong and C. G. Dick, et al., Arthroscopic reduction and percutaneous fixation of selected calcaneus fractures: Surgical technique and early results, *J. Orthop. Trauma.,* **28** (2014), 569–576.
6. A. A. Abdelgawad and E. Kanlic, Minimally invasive (sinus tarsi) approach for open reduction and internal fixation of intra-articular calcaneus fractures in children: Surgical technique and case report of two patients, *J. Foot. Ankle. Surg.,* **54** (2015), 135–139.
7. M. Ni, J. Mei and K. Li, et al., The primary stability of different implants for intra-articular calcaneal fractures: An in vitro study, *Biomed. Eng. Online.,* **17** (2018), 50.
8. Ihab I. El-Desouky and W. Abu Senna, The outcome of super-cutaneous locked plate fixation with percutaneous reduction of displaced intra-articular calcaneal fractures, *Injury.,* **48** (2017), 525–530.
9. C. H. Park and D. H. Yoon, Role of Subtalar Arthroscopy in Operative Treatment of Sanders Type 2 Calcaneal Fractures Using a Sinus Tarsi Approach, *Foot. Ankle. Int.,* **39** (2018), 443–449.
10. T. Zhang, Y. Su and W. Chen, et al., Displaced intra-articular calcaneal fractures treated in a minimally invasive fashion: Longitudinal approach versus sinus tarsi approach, *J. Bone. Joint. Surg. Am.,* **96** (2014), 302–309.
11. J. H. Yeo, H. J. Cho and K. B. Lee, Comparison of two surgical approaches for displaced intra-articular calcaneal fractures: Sinus tarsi versus extensile lateral approach, *BMC. Musculoskeletal. Disord.,* **16** (2015), 63.
12. H. C. Zhou, T. Yu and H. Y. Ren, et al., Clinical Comparison of Extensile Lateral Approach and Sinus Tarsi Approach Combined with Medial Distraction Technique for Intra-Articular Calcaneal Fractures, *Orthop. Surg.,* **9** (2017), 77–85.
13. M. Ni, D. W. C. Wong and J. Mei, et al., Biomechanical comparison of locking plate and crossing metallic and absorbable screws fixations for intra-articular calcaneal fractures, *Sci. China. Life. Sci.,* **59** (2016), 958–964.
14. I. L. Gitajn, M. Abousayed and R. J. Toussaint, et al., Anatomic Alignment and Integrity of the Sustentaculum Tali in Intra-Articular Calcaneal Fractures: Is the Sustentaculum Tali Truly Constant? *J. Bone. Joint. Surg. Am.,* **96** (2014), 1000–1005.
15. A. R. Hsu, R. B. Anderson and B. E. Cohen, Advances in Surgical Management of Intra-articular Calcaneus Fractures, *J. Am. Acad. Orthop. Surg.,* **23** (2015), 399–407.

16. B. Swartman, D. Frere and W. Wei, et al., Wire Placement in the Sustentaculum Tali Using a 2D Projection-Based Software Application for Mobile C-Arms: Cadaveric Study, *Foot. Ankle. Int.*, **39** (2018), 485–492.
17. P. P. Lin, S. Roe and M. Kay, et al., Placement of screws in the sustentaculum tali. A calcaneal fracture model, *Clin. Orthop. Relat. Res.*, (1998), 194–201.
18. C. Wang, D. Huang and X. Ma, et al., Sustentacular screw placement with guidance during ORIF of calcaneal fracture: An anatomical specimen study, *J. Orthop. Surg. Res.*, **12** (2017), 78.
19. A. T. Scott, D. A. Pacholke and K. S. Hamid, Radiographic and CT Assessment of Reduction of Calcaneus Fractures Using a Limited Sinus Tarsi Incision, *Foot. Ankle. Int.*, **37** (2016), 950–957.
20. K. J. Chung, D. Y. Hong and Y. T. Kim, et al., Preshaping plates for minimally invasive fixation of calcaneal fractures using a real-size 3D-printed model as a preoperative and intraoperative tool, *Foot. Ankle. Int.*, **35** (2014), 1231–1236.
21. A. R. Hsu and J. K. Ellington, Patient-Specific 3-Dimensional Printed Titanium Truss Cage With Tibiotalocalcaneal Arthrodesis for Salvage of Persistent Distal Tibia Nonunion, *Foot. Ankle. Spec.*, **8** (2015), 483–489.
22. J. R. Jastifer and P. A. Gustafson, Three-Dimensional Printing and Surgical Simulation for Preoperative Planning of Deformity Correction in Foot and Ankle Surgery, *J. Foot. Ankle. Surg.*, **56** (2017), 191–195.
23. W. Zheng, M. D. Zhenyu Tao and M. D. Yiting Lou, et al., Comparison of the Conventional Surgery and the Surgery Assisted by 3d Printing Technology in the Treatment of Calcaneal Fractures, *J. Invest. Surg.*, (2017), 1–11.
24. T. Kurozumi, Y. Jinno and T. Sato, et al., Open reduction for intra-articular calcaneal fractures: Evaluation using computed tomography, *Foot. Ankle. Int.*, **24** (2003), 942–948.
25. H. B. Kitaoka, I. J. Alexander and R. S. Adelaar, et al., Clinical rating systems for the ankle-hindfoot, midfoot, hallux, and lesser toes, *Foot. Ankle. Int.*, **15** (1994), 349.
26. M. Freyd, The Graphic Rating Scale, *J. Educ. Psychol.*, **14** (1923), 83–102.
27. B. W. Bussewitz and C. F. Hyer, Screw placement relative to the calcaneal fracture constant fragment: An anatomic study, *J. Foot. Ankle. Surg.*, **54** (2015), 392–394.
28. M. Qiang, Y. Chen and K. Zhang, et al., Effect of sustentaculum screw placement on outcomes of intra-articular calcaneal fracture osteosynthesis: A prospective cohort study using 3D CT, *Int. J. Surg.*, **19** (2015), 72–77.
29. J. Geerling, D. Kendoff and M. Citak, et al., Intraoperative 3D imaging in calcaneal fracture care-clinical implications and decision making, *J. Trauma.*, **66** (2009), 768–773.
30. R. Kakwani and M. Siddique, Operative compared with nonoperative treatment of displaced intra-articular calcaneal fractures: A prospective, randomized, controlled multicenter trial, *J. Bone. Joint. Surg. Am.*, **84** (2002), 1733–1744.
31. A. H. Ragab, I. M. Mubark and A. M. Nagi, et al., Treatment of subtalar calcanean fractures using trans-osseous limited lateral approach, *Ortop. Traumatol. Rehabil.*, **16** (2014), 629–638.